



HAL
open science

3D numerical modeling of a new thermo-inductive NDT using pulse mode and pulsed phase methods

B. Ramdane, D. Trichet, M. Belkadi, T. Saidi, J. Fouladgar

► To cite this version:

B. Ramdane, D. Trichet, M. Belkadi, T. Saidi, J. Fouladgar. 3D numerical modeling of a new thermo-inductive NDT using pulse mode and pulsed phase methods. *European Physical Journal: Applied Physics*, 2010, 52 (2), 10.1051/epjap/2010049 . hal-00634375

HAL Id: hal-00634375

<https://hal.science/hal-00634375>

Submitted on 21 Oct 2011

HAL is a multi-disciplinary open access archive for the deposit and dissemination of scientific research documents, whether they are published or not. The documents may come from teaching and research institutions in France or abroad, or from public or private research centers.

L'archive ouverte pluridisciplinaire **HAL**, est destinée au dépôt et à la diffusion de documents scientifiques de niveau recherche, publiés ou non, émanant des établissements d'enseignement et de recherche français ou étrangers, des laboratoires publics ou privés.

3D numerical modeling of a new thermo-inductive NDT using pulse mode and pulsed phase methods

B. Ramdane, D. Trichet, M. Belkadi and J. Fouladgar
Institut de Recherche en Electrotechnique et Electronique de Nantes Atlantique (IREENA)
37, Boulevard de l'université – BP 406 – 44600 Saint Nazaire Cedex, France
E-mail: brahim.ramdane@univ-nantes.fr

Abstract. Thermo-inductive testing is a new technique used for health inspection on different components of automotive and aeronautic industries. Defect detection is based on the modification of induced eddy current and temperatures due to the presence of defects. The temperature change propagated at the surface of the specimen can then be detected by an infrared camera. In this work, a 3D numerical model of this technique is developed and applied to aeronautic materials. Results obtained are compared with the infrared thermography method to demonstrate the relevance of the new technique.

PACS. 02.70.Dh Finite-element and Galerkin methods - 81.70.Ex Non destructive testing: electromagnetic testing, eddy-current testing - 44.00.00 Heat transfer

1. Introduction

Cracks constitute one of the major problems threatening the security of systems subjected to mechanical, thermal or chemical constraints. Their detection and characterization then assume a great importance. When it concerns a control without affecting the integrity of the inspected material, Non Destructive Techniques (NDT) are generally used. Many methods of NDT are in a constant development according to applications and investigation fields. One can give as example the infrared thermography and the eddy current testing. These techniques are more or less effective depending on the nature, the geometry and the physical properties of the inspected materials and the defects.

In the aeronautic industry, the most observed defects are the microcracks in aluminium plates and the cracks or delaminations inside composite materials. These defects can be generated either during manufacturing or during the life cycle. For example, drilling before riveting can produce different imperfections in the structure which are not easily detectable by classical techniques.

In this context, we propose a new method called thermo-inductive technique which combines the advantages of both eddy current and infrared thermography techniques. In this method, the electrical conducting material to be inspected is placed in an alternative field generated by a suitable inductor. The currents induced in the material are deviated by defects. This deviation creates high induced power concentration leading to local superheating around the default. After a given exposition time, the temperature anomaly is propagated to the material surface, and can be detected by an infrared camera [1-2]. In this technique, the defects are more or less detectable depending on the depth penetration of the induced currents, the type of the defect, the duration of heating, the position and the inductor geometry.

Till now, the development of this new technique has been specially carried out by experimental researches. Improvement and optimization of the technique need however a thorough theoretical investigation. Due to the complexity of the system and the nature of the defects, this stage of investigation should be done by a 3D numerical modeling. For this purpose, we have developed a 3D finite element method based on Whitney's elements under a Matlab environment as a support tool to model the different phenomena involved in this technique. These models also take into account the anisotropy of materials and are validated by comparison with experimental data and workshop problems.

The new technique is applied on defects detection in the case of a post drilling operations in aluminium and carbon fiber composite plates. A comparison with the classical infrared thermography method has also been done to demonstrate the interest of the new technique. Investigations on various parameters such as inductor geometry, default characteristics (size, depth) and field frequency have been carried out in order to study the efficiency and the feasibility of the technique.

2. Problem description

A typical measurement installation for the thermo-inductive technique is shown in Figure 1. It consists of an induction generator, an inductor, a piece to be inspected, and an infrared camera to detect and record the surface temperatures. According to the application, a working frequency interval between 50Hz and 2 MHz may be used.

The study of this technique involves both thermal and electromagnetic phenomena. The aim of numerical modeling is to determine the magnetic field created by the inductor and to deduce the induced currents and the local power losses by Joule

effect in the piece. Then, the temperature is calculated by using this power dissipation which is the coupling term of magneto-thermal problem.

3. Numerical modeling

3.1 Electromagnetic model

3.1.1 Studied problem

The electromagnetic problem can be described as shown in Figure 2. The whole domain contains a current source, a conducting region Ω_c , a region with magnetic material, and an air box Ω . In linear time harmonic state, the Maxwell's equations become [4]:

$$\mathbf{Curl}\mathbf{E} = -j\omega\mathbf{B} \quad (1)$$

$$\mathbf{Curl}\mathbf{H} = \mathbf{J}_s + \mathbf{J}_{ind} \quad (2)$$

Where \mathbf{E} represents the electric field, \mathbf{B} the magnetic flux density, \mathbf{H} the magnetic field, and \mathbf{J}_{ind} the eddy current in Ω_c .

The boundary conditions will be ensured by:

$$\mathbf{B} \cdot \mathbf{n}|_{\Gamma_b} = 0 \quad \text{and} \quad \mathbf{H} \times \mathbf{n}|_{\Gamma_H} = 0 \quad (3)$$

To complete the problem, constitutive laws have been introduced under the following form:

$$\mathbf{B} = [\mu(\mathbf{H})] \cdot \mathbf{H} \quad \text{and} \quad \mathbf{J}_{ind} = [\sigma] \cdot \mathbf{E} \quad (4)$$

Where $[\mu]$ represents the tensor of magnetic permeabilities, and $[\sigma]$ the tensor of electric conductivities.

3.1.2 The electric formulation

As the magnetic field density is divergence free, a magnetic vector potential \mathbf{A} can be introduced. Using (1), the electric field in Ω_c can be written as a function of \mathbf{A} and the electric scalar potential V [4-6]:

$$\mathbf{E} = -(j\omega\mathbf{A} + \mathbf{grad}V) \quad (5)$$

The local Faraday and Ampere laws can be written as:

$$\mathbf{Curl}([\mu]^{-1} \cdot \mathbf{Curl}\mathbf{A}) + [\sigma] \cdot (j\omega\mathbf{A} + \mathbf{grad}V) = \mathbf{J}_s \quad (6)$$

$$\text{div}[-[\sigma] \cdot (j\omega\mathbf{A} + \mathbf{grad}V)] = 0 \quad (7)$$

Applying the weighted residual method with the edge test function \mathbf{W}_e and nodal test function \mathbf{W}_n and taking into account the boundary conditions, we have:

$$\int_{\Omega} [\mathbf{Curl}([\mu]^{-1} \cdot \mathbf{Curl}\mathbf{A}) + j\omega[\sigma] \cdot (\mathbf{A} + \mathbf{grad}\phi)] \cdot \mathbf{W}_e \cdot d\Omega = \int_{\Omega} \mathbf{J}_s \cdot \mathbf{W}_e \cdot d\Omega \quad (8)$$

$$\int_{\Omega} [\text{div}[\sigma] \cdot j\omega(\mathbf{A} + \mathbf{grad}\phi)] \cdot \mathbf{W}_n \cdot d\Omega = 0 \quad (9)$$

where $j\omega\phi = V$.

In order to enforce $\text{div}\mathbf{J} = 0$, we express \mathbf{J} by $\text{Curl}\mathbf{T}_s$ in the conducting domain, where \mathbf{T}_s is the electrical vector potential which replaces the source field [7].

3.2 Thermal model

The thermal problem is defined by heat transfer equation:

$$\rho C_p \frac{\partial T}{\partial t} + \text{div}(-[\lambda] \cdot \mathbf{grad} T) = P \quad (10)$$

Where T , ρ , C_p , $[\lambda]$ are respectively, the temperature, the specific mass, the specific heat, the thermal conductivity. P is the induced power density calculated with the electromagnetic problem expressed by:

$$P = \mathbf{J}_{\text{ind}}^T [\sigma]^{-1} \cdot \mathbf{J}_{\text{ind}} \quad (11)$$

The boundary conditions are described by convection from the object free surfaces as:

$$-[\lambda] \frac{\partial T}{\partial \mathbf{n}} \Big|_{\Gamma_c} = h_{\text{cv}} \cdot (T - T_a) \quad (12)$$

Where T_a is the ambient temperature, and h_{cv} the convective heat transfer coefficient.

In thermo-inductive technique, as in the infrared thermography testing, there are various modes for thermal stimulation: pulse or modulated excitation [8].

In the first mode, a pulse of energy is injected in the specimen and propagates in the material. The duration of the pulse is variable depending on the thickness of the material to be evaluated and its thermal properties. The thermal problem is thus defined by (10).

The variational formulation is established by solving (10):

$$\int_{\Omega} \left[\rho C_p \frac{\partial T}{\partial t} - \text{div}([\lambda] \cdot \mathbf{grad} T) \right] \cdot W_n \cdot d\Omega = \int_{\Omega} P \cdot W_n \cdot d\Omega \quad (13)$$

In the second mode of stimulation, the specimen is submitted to a sinusoidal modulated power [8]. The time variation term becomes:

$$\frac{\partial}{\partial t} = j\omega_{\text{th}} \quad (14)$$

Where ω_{th} is the modulating frequency of the heating source. Equation (10) becomes:

$$j \rho C_p \omega_{\text{th}} \cdot T + \text{div}(-[\lambda] \cdot \mathbf{grad} T) = P \quad (15)$$

In this paper, we focus on the pulse stimulation, because it is easier to implement and it has a faster response.

3.3 Discretization

Both electric and thermal formulations have been solved using finite element method. In 3D, using the Whitney's elements, four discrete spaces can be introduced: the nodal element space, the edge element space, the facet element space, and the volume element space [5]. According to their properties, Φ and T are interpolated by the nodal elements, and \mathbf{A} and \mathbf{T}_s by the edge elements [7].

As the temperature variation interval is relatively small, the parameters of electromagnetic and thermal problems are set for this range of temperature.

The system has been solved by the conjugate gradient method. For the electromagnetic formulation, it has been shown that the use of a tree gauge condition to ensure the uniqueness of \mathbf{A} is not necessary if we use the compatible formulation [7]. The anisotropic properties are taken into account in the developed code by involving electrical conductivity, thermal conductivity and magnetic permeability tensors [11].

4. Model validation

Numerical models developed for NDT by thermo-inductive technique have been evaluated as a support tool for the qualification of the detection process. To have a good detection, the influence of the defect on the current density has to be high enough to provide an infrared signal stronger than neighbouring temperatures.

The first step is to validate the finite element model by comparison with experimental data. Figure 3 shows the experimental device of the thermo-inductive technique. In order to validate our numerical models, the technique was carried out on a ferromagnetic piece whose dimensions are shown in the Figure 4(a). A surface crack with a depth of 2.5 mm, length of 20 mm and width of 0.1 mm was inserted in the specimen excited by an electromagnetic field at a frequency of 50 Hz.

The presence of the defect creates the concentration of induced current at the extremities of the default as shown in Figure 4(b).

Figure 5 illustrates the temperature field around the default obtained by infrared camera. The presence of the defect generates two hot spots at the defect's extremities. These hot regions are best illustrated in Figure 6 where the measured temperature is plotted along the defect axis. On the same figure the simulation results are compared with experimental data. A good concordance between the two curves is observed. The difference is partly due to the noise in the measurement and variation of the material emissivity.

5. Applications and results

In order to study the defect detection and the influence of various parameters of the system on the characterization of the crack, it is necessary to introduce a discriminating parameter.

In the case of pulse stimulation, thermal contrast analysis provides a good indication of defect characteristics. Several definitions have been proposed for the contrast evaluation. In the "pulse mode method" one uses the normalized thermal contrast defined by:

$$C_i(t) = \frac{T_{\text{def}}(t) - T_{\text{def}}(t_0)}{T_{\text{sdef}}(t) - T_{\text{sdef}}(t_0)} \quad (16)$$

Where $C_i(t)$ is the normalized thermal contrast in a point (i) at time t . T_{def} , T_{sdef} are surface temperatures with and without defect in a point (i), and t_0 is the initial time. It can be noticed that the more the thermal contrast is different from 1 the better the defect detection is.

5.2 Comparison with infrared thermography

In this section, a comparison between the thermo-inductive technique and the classical infrared thermography is carried out for the aeronautic application defined in II. Figure 7 shows a cut on the plane YOZ of the studied piece, it is a drilled aluminium plate with a lateral defect.

We have calculated the thermal contrast C_i for a heating period of 2 seconds. Two types of inductors are used for this simulation: an inductor of the form U along X axis and another of circular form with Z axis. The cartography of C_i for the first form of inductor (Fig. 8) shows that the temperature is more contrasted around the defect and propagates to the surface plate.

Figure 9 shows the evolution of the thermal contrast calculated from the numerical model versus the heating period. In the case of short heating period and high frequencies, the thermal contrast is larger than 1. With increasing heating time duration, the contrast becomes smaller, which means that the additional temperature around the crack decreases. This is mainly due to the diffusion of heat by conduction in the material. It can be concluded that the thermal contrast is decreasing with the heating duration. In practice, a heating time of about 0.5 second is a good compromise between the infrared camera detection level, the generator capacity and the thermal contrast.

One can notice that the use of thermo-inductive technique increases the contrast compared to the one obtained by infrared thermography method for the same total power injected in the plate. This improvement is more interesting when one looks at the evolution of temperature difference in Figure 10 where it is multiplied by ten.

One can also observe that the design of the inductor has a great influence on the performance of the system. Indeed, inductor of the form U gives better results than the circular one. This result is interesting because it shows that with our numerical models, we have the possibility to optimize the design of the inductor (form, size,...) with a goal function based on the contrast.

In order to deepen this comparison, we have studied the defect detection for the same plate with another crack configuration. It consists of a vertical crack with the dimensions given in Figure 11. In this case, the crack becomes undetectable with the infrared thermography (Thermal contrast equal to 1). However, the use of thermo-inductive method improves considerably the defect detection as shown in the Figure 12.

5.3 Investigation on the system performance

The results obtained show the advantage of the new technique. The next step will be the investigations on various parameters of the method to optimize the system performance.

5.3.1 Phase contrast

The use of the “pulse mode” as a characterization tool is not sufficient because the thermal contrast C_i defined in (16) depends on the induced power which may be non uniform inside the piece. To complete the characterization tool, a new approach called “pulsed phase method” is proposed. This technique combines simultaneously the advantages of both pulse and modulated stimulations. The specimen is pulse heated by induction and the phase of the thermal waves induced in the specimen is obtained by the Fourier’s transform of the temperature evolution.

If this approach is carried out, the phase contrast is used to quantify the defect detectability. After the initial thermal pulse, the temporal evolution $s(t)$ of the surface temperature is calculated and extracted for each pixel. Then, the discrete Fourier’s transform is computed according to the well-known formula:

$$F(f) = \Delta t \cdot \sum_{n=0}^{N-1} s(t) \cdot \exp(-j2\pi fn\Delta t) = R(f) + jI(f) \quad (17)$$

Where $R(f)$ and $I(f)$ are respectively, the real and imaginary components of $F(f)$ and Δt is the sampling time step. Finally, the phase is computed for each of the transformed terms using:

$$\Phi(f) = \tan^{-1} \left(\frac{I(f)}{R(f)} \right) \quad (18)$$

and the phase contrast is defined by:

$$\Delta\Phi_i = \Phi_{\text{def}} - \Phi_{\text{sdef}} \quad (19)$$

Where $\Delta\Phi_i$ is the phase contrast in a point (i). Φ_{def} , Φ_{sdef} are phases with and without defect in the same point (i).

The phase contrast is often used due to its sensitivity to the thermo physical property (the depth of the defect and the source thermal frequency). This parameter has also the advantage of being less sensitive to non uniform heating.

5.3.2 Skin depth and heating duration

It is shown, that depending on the material and defect properties, on the excitation frequency and on the duration of the heating pulse, one gets higher or lower thermal contrasts.

To evaluate the defect detectability as a function of the skin depth and crack depth, we have calculated the surface temperature for the defects of the Figures 7 and 11. Figures 13 to 16 show the thermal and phase contrast for a heating period of two seconds for different skin depths.

We notice that the defect detectability is better at frequencies where the skin depth is greater than or equal to the crack’s depth. Indeed, for the lower frequencies, the heating is practically uniform in the volume and consequently the surface temperature is less sensitive to defect.

The phase contrast gives the same results (Figs. 14 and 16). One remarks that by increasing the excitation frequency, the thermal contrast passes by a maximum which corresponds to an optimal value of the induction frequency. It should be noted that for materials with low electrical conductivity, it is necessary to raise the working frequency range. From Figures 14 and 16, it can be observed that an optimum thermal frequency exists for which a defect produces a maximum phase contrast.

5.3.3 Crack thickness

Another important parameter is the defect thickness. The figures 17 and 18 show that the thermal and phase contrasts increase with the defect thickness. This result indicates that these contrasts could be used to discriminate the crack’s dimensions.

5.4 Application to composite material

In this case, the plate inspected is a carbon fiber reinforced composite with the same dimensions shown in Figure 7. It is an anisotropic material with physical characteristics given in Table 1. The anisotropy is taken into account by involving electrical and thermal conductivities tensors. The electrical conductivity is equal to zero following the depth because the layers are separated by an insulating resin.

We have calculated the thermal and phase contrast (Figs. 19 and 20) for a heating period of 2 seconds. The composite have relatively low thermal conductivity in their depth direction. As a consequence, the thermal contrast reaches its maximum value some fraction of seconds after turning off of the power source.

The results give a good indication of how the composite material responds to thermal excitation. These materials have a low electrical conductivity. Therefore to obtain an acceptable level of contrast, one should use high frequencies upper to 1 MHz. As in the case of aluminum plates, the maximum thermal and phase contrast values increase with the induction frequency.

6. Conclusion

In this paper, the thermo-inductive technique has been studied in order to detect defects in aeronautic materials. The temperature contrast at the surface of the specimen generated by eddy currents was measured for this purpose. A 3D numerical coupled model using Whitney's elements was developed and applied to compute induced currents and temperature distribution in the inspected piece. Experimental data have enabled us to validate finite element models. The pulse stimulation has been studied due to its facility of implementation and its rapid response. Two complementary discrimination parameters are defined to analyze the results. The first one, pulse mode, is adapted to homogenized heating and the second one, pulsed phase, which is less sensitive to non uniform induced power.

A comparison of contrasts with those obtained using the classical infrared thermography method shows that the new technique is more interesting in term of defect detection for electrical conducting materials.

The simulation results show that the crack detection depends on the inductor geometry, the heating duration, the excitation frequency and the defect size. They have demonstrated the relevance of the thermo-inductive technique and the efficiency of 3D model. It should be noticed that, the 3D numerical system is very difficult to inverse. It is not well suited for real time operations. It can be however used to obtain the abacus or the tables for different defects. In this case, the inversion can be obtained faster.

References

1. B. Ramdane, D. Trichet, M. Belkadi, J. Fouladgar and T. Saidi, in *Proceedings of 13th IEEE CEFC, Athens, Greece (Mai 2008)*.
2. G. Walle, U Netzelmann, in *Proceedings of 9th European Conference on Non-Destructive Testing (ECNDT 2006)*, (Berlin, Germany, 2006)
3. B. OSWALD-TRANTA, G. WALLY, in *Proceedings of 9th European Conference on Non-Destructive Testing (ECNDT 2006)*, (Berlin, Germany 2006)
4. O. Biro, K. Pries, *IEEE Trans. Magn.* **25**, 3145 (1989)
5. A. Bossavit, *IEEE Trans. Magn.* **24**, 74 (1988)
6. T. Henneron, Y. Le Menach, F. Piriou, O. Moreau, S. Clénet, J.-P. Vértité, *IEEE Trans. Magn.* **41**, 1785 (2007)
7. Z. Ren, *IEEE Trans. Magn.* **32**, 6555 (1996)
8. C. Ibarra-Castanedo, Ph.D thesis, University of Laval Quebec, 2005
9. X. Maldague, S. Marinetti, *Eur. Appl. J. Appl. Phys.* **79**, 2694 (1996)
10. T. Sakagami, S. Kubo, *Infrared Physics & Technology* **43**, 211 (2002)
11. J. P. A. Bastos and N. Sadowski, *Electromagnetic modelling by finite element methods* (Marcel Dekker, New York, 2003)

Figure captions

Fig. 1. Schematic of studied system

Fig. 2. Studied Domain

Fig. 3. Experimental setup

Fig. 4. (a) Modeled piece with crack and (b) Real part of the current density distribution

Fig. 5. Experimental temperature distribution

Fig. 6. Simulated and measured temperature distribution along the defect axis after 0.5 second

Fig. 7. Dimensions of the drilled plate (crack width 1.5mm)

Fig. 8. Image of thermal contrast distribution

Fig. 9. Thermal contrast as a function of the heating time (Heating period 2s, fr=20kHz)

Fig. 10. Temperature difference as a function of the heating time (Heating period 2s, fr=20kHz)

Fig. 11. Dimensions of the drilled plate (crack thickness 0.1mm)

Fig. 12. Thermal contrast as a function of the heating time (Heating period 2s, fr=8kHz)

Fig. 13. Thermal contrast as function of the heating duration for different skin depth (horizontal defect)

Fig. 14. Phase contrast as function of the thermal frequency for different skin depth (horizontal defect)

Fig. 15. Thermal contrast as function of the heating duration for different skin depth (vertical defect)

Fig. 16. Phase contrast as function of the thermal frequency for different skin depth (vertical defect)

Fig. 17. Thermal contrast as function of the heating duration for different crack thickness

Fig. 18. Phase contrast as function of the thermal frequency for different crack thickness

Fig. 19. Thermal contrast as function of the heating duration for different excitation frequency

Fig. 20. Phase contrast as function of the thermal frequency for different excitation frequency

Table captions

Table 1. Physical properties of composite material

Figures

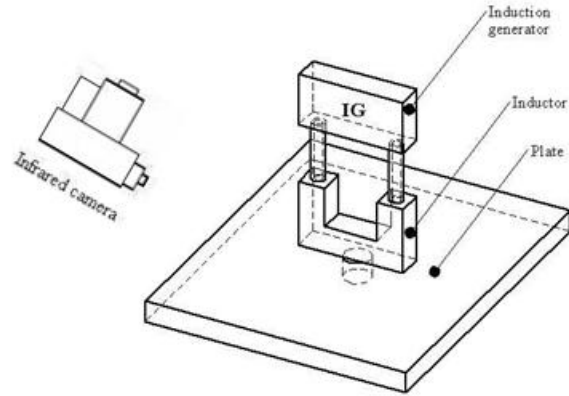


Fig. 1. Schematic of studied system

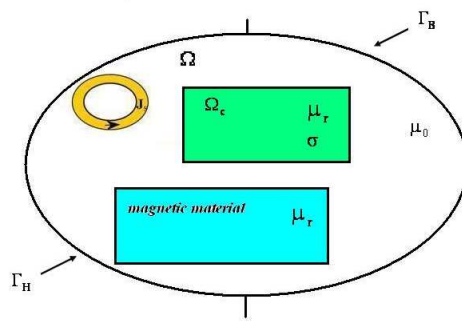


Fig. 2. Studied Domain

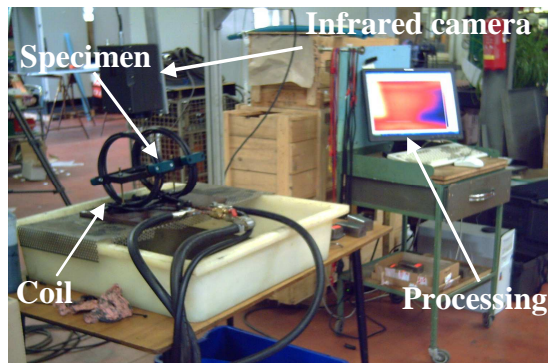


Fig. 3. Experimental setup

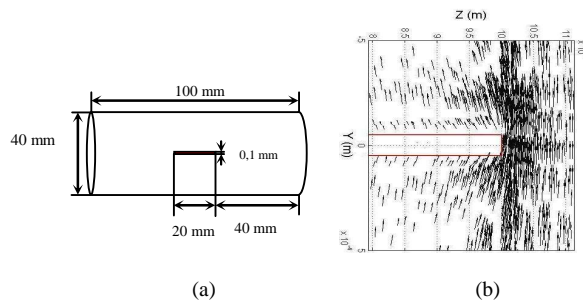


Fig. 4. (a) Modeled piece with crack and (b) Real part of the current density distribution

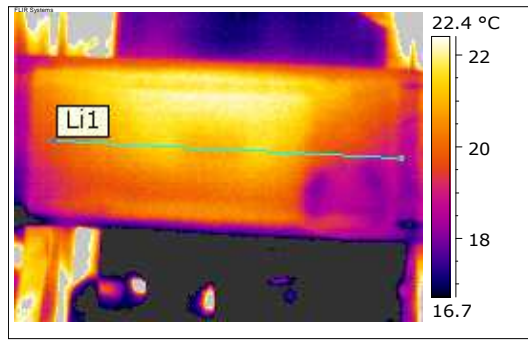


Fig. 5. Experimental temperature distribution

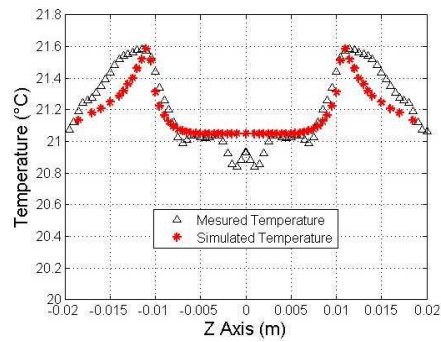


Fig. 6. Simulated and measured temperature distribution along the defect axis after 0.5 second

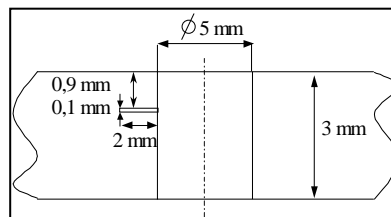


Fig. 7. Dimensions of the drilled plate (crack width 1.5mm)

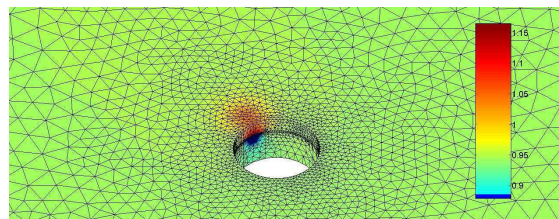


Fig. 8. Image of thermal contrast distribution

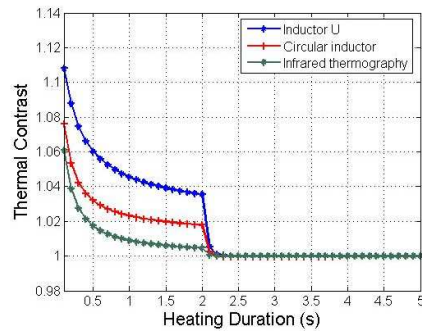


Fig. 9. Thermal contrast as a function of the heating time (Heating period 2s, fr=20kHz)

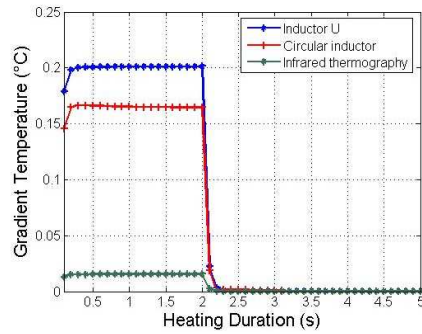


Fig. 10. Temperature difference as a function of the heating time (Heating period 2s, fr=20kHz)

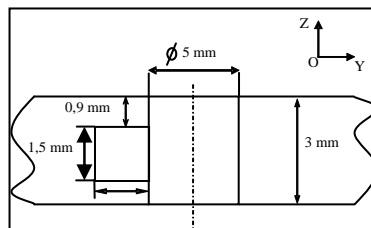


Fig. 11. Dimensions of the drilled plate (crack thickness 0.1mm)

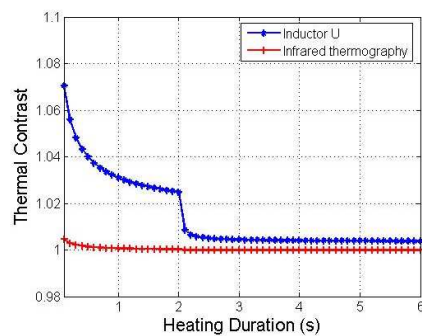


Fig. 12. Thermal contrast as a function of the heating time (Heating period 2s, fr=8kHz)

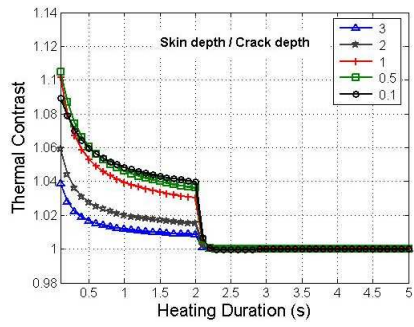


Fig. 13. Thermal contrast as function of the heating duration for different skin depth (horizontal defect)

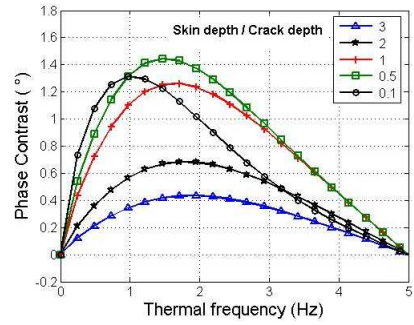


Fig. 14. Phase contrast as function of the thermal frequency for different skin depth (horizontal defect)

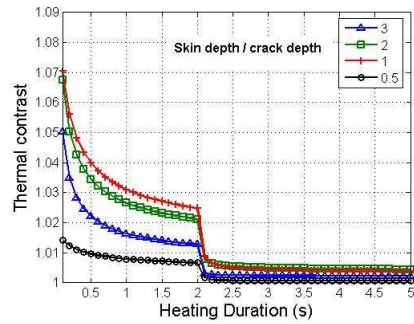


Fig. 15. Thermal contrast as function of the heating duration for different skin depth (vertical defect)

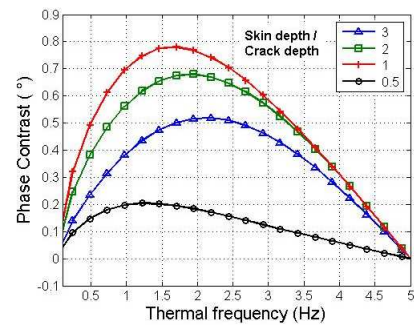


Fig. 16. Phase contrast as function of the thermal frequency for different skin depth (vertical defect)

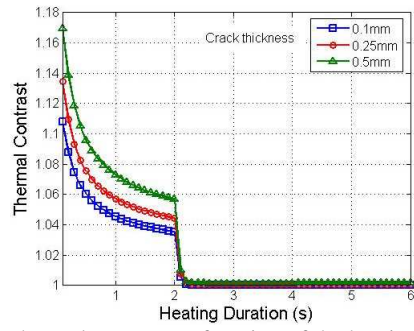


Fig. 17. Thermal contrast as function of the heating duration for different crack thickness

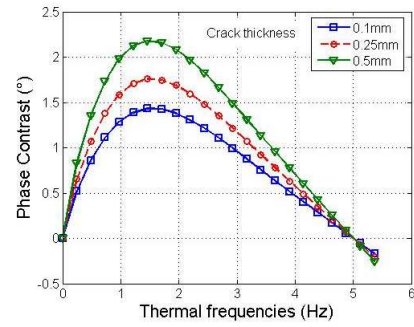


Fig. 18. Phase contrast as function of the thermal frequency for different crack thickness

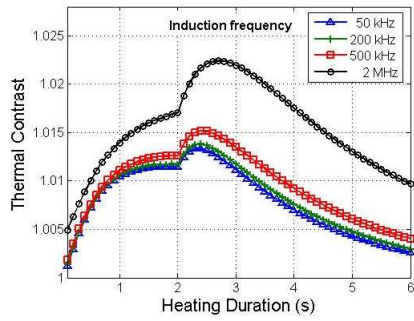


Fig. 19. Thermal contrast as function of the heating duration for different excitation frequency

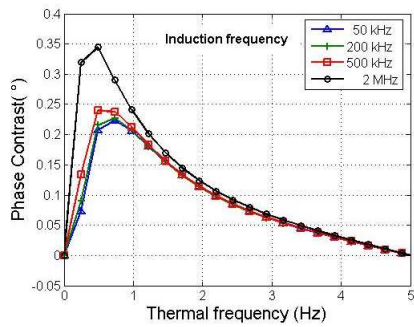


Fig. 20. Phase contrast as function of the thermal frequency for different excitation frequency

Tables

Table 1. Physical properties of composite material

Electrical Conductivity ($S.m^{-1}$)		Thermal Conductivity ($W.m^{-1}K^{-1}$)		Specific Heat ($Jkg^{-1}K^{-1}$)	Density ($Kg.m^{-3}$)
X & Y axes	Z axis	X & Y axes	Z axis		
20 000	0	3	0.45	1280	1600